

Interferometric Imaging of Geostationary Satellites: Signal-to-Noise Considerations

Anders M. Jorgensen^a, H. R. Schmitt^{b,c}, D. Mozurkewich^d, J. T. Armstrong^b,
S. Restaino^b, R. L. Hindsley^b

^aNew Mexico Institute of Mining and Technology, Socorro, NM, USA

^bNaval Research Laboratory, Washington, DC, USA

^cComputational Physics Inc, Springfield, VA

^dSeabrook Engineering, Seabrook, MD, USA

ABSTRACT

Geostationary satellites are generally too small to image at high resolution with conventional single-dish telescopes. Obtaining many resolution elements across a typical geostationary satellite body requires a single-dish telescope with a diameter of 10's of m or more, with a good adaptive optics system. An alternative is to use an optical/infrared interferometer consisting of multiple smaller telescopes in an array configuration. In this paper and companion papers^{1,2} we discuss the performance of a common-mount 30-element interferometer. The instrument design is presented by Mozurkewich et al.,¹ and imaging performance is presented by Schmitt et al.² In this paper we discuss signal-to-noise ratio for both fringe-tracking and imaging. We conclude that the common-mount interferometer is sufficiently sensitive to track fringes on the majority of geostationary satellites. We also find that high-fidelity images can be obtained after a short integration time of a few minutes to a few tens of minutes.

1. INTRODUCTION

While the U.S. has telescopes around the world capable of imaging objects in low-Earth orbit (LEO), the capability to image high-altitude satellites in the visible and near-infrared still does not exist, and is needed to support the Space Situational Awareness (SSA) mission. GEO satellites are typically very large, very high value, sometimes exceeding $> \$10^9$, providing essential military and civilian communications services (such as satellite TV signal and other communications). In previous papers^{3,4} we discussed the possibility of imaging satellites with astronomical interferometers. In this paper, two companion papers,^{1,2} as well as two recent papers^{5,6} we examine satellite imaging with a common-mount interferometer consisting of thirty 1.4 m telescopes.

Geostationary satellites have a size of a few 10s of m, and the desired resolution is often a fraction of a m.^{3,4,7} To achieve the desired resolution with a single-dish telescope would require a diameter of several 10s of m to close to 100 m. Such a large telescope would be extremely expensive, would require a very sophisticated adaptive optics system, and would be overkill in terms of its photon collection capability.

An alternative is to use a interferometer. We propose a common-mount interferometer which involves a large number of individual telescopes mounted on a sin-

gle steerable platform. There are several advantages to this, including that it eliminates the need for long delay lines, and eliminates the need for mounts on the individual telescopes. That in turn reduces complexity and allows for the telescopes to be placed closer together to achieve shorter baselines which are necessary for geostationary satellite imaging.³

Geostationary satellites are also faint. Their median brightness is V=13.5, with some as bright as V=10 and a few fainter than V=15.^{4,8} That satellites are faint and large poses fringe-tracking and imaging SNR questions which must be explored. We do that in this paper.

The Navy Prototype Optical Interferometer⁹ (NPOI) has demonstrated the phasing of an optical baseline on a GEO source using a specular reflection of sunlight from the source.^{7,10,11} The Magdalena Ridge Observatory Interferometer (MROI) has been proposed as a satellite imaging interferometer because of its planned short baselines and large apertures.^{4,12} While MROI is expected to track fringes on targets as faint as geostationary satellites, both NPOI and MROI suffer from baselines which are too long for optimal tracking on the very large satellite objects.³ NPOI has the capability for much shorter baselines, but has smaller apertures with limited light collection. MROI cannot observe shorter baselines because of the size of telescopes and their enclosures.

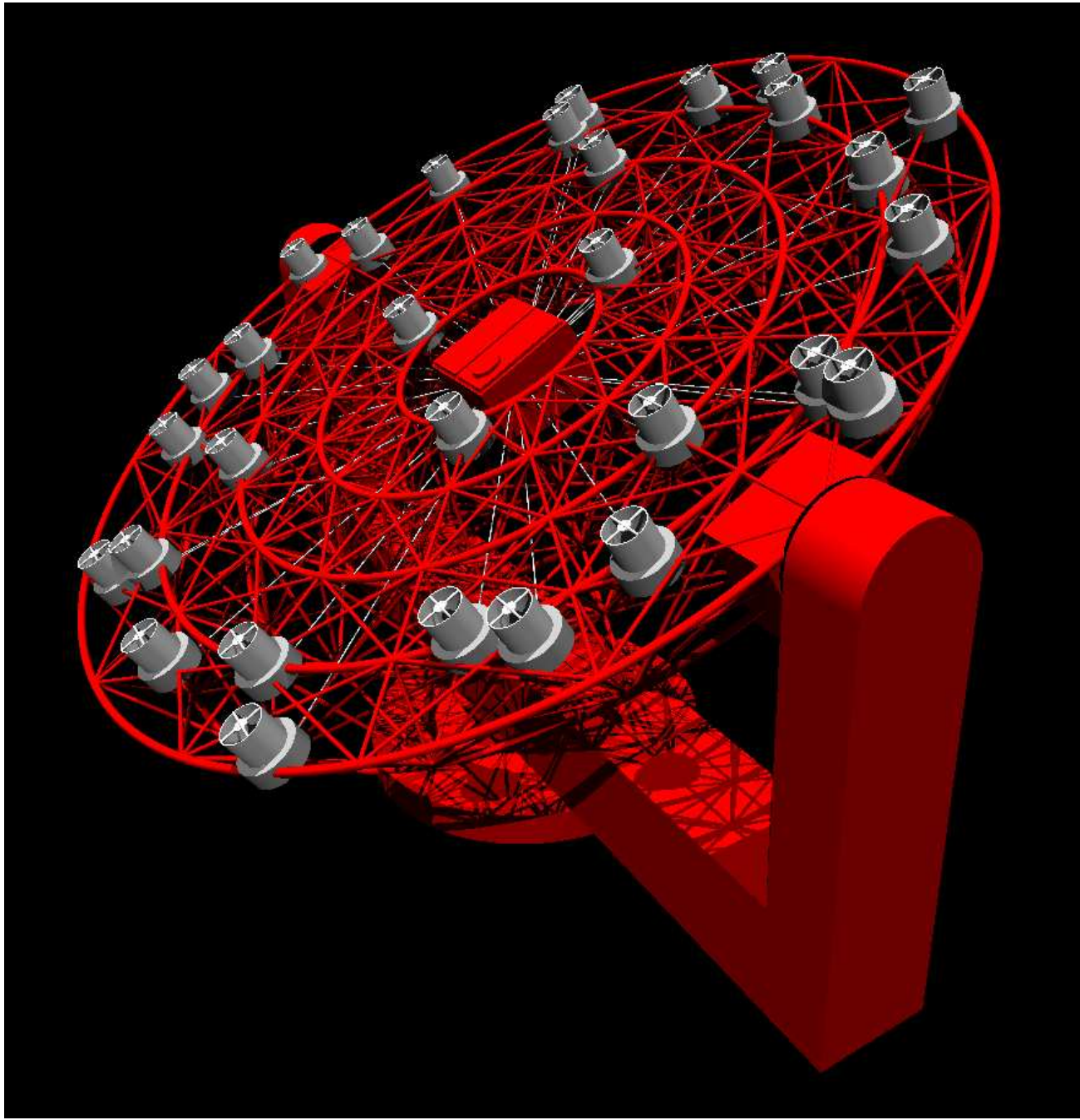


Figure 1. Three-dimensional model of the instrument. 30 telescopes are mounted on an Alt-Az platform. In the model the individual telescopes can be seen, as well as the fiber relay pipes to the combiner room, and the combiner room.

The Geo Light Imaging National Testbed¹³ (GLINT) is an imaging concept in which the geostationary satellite is flood illuminated by 3 lasers simultaneously. Pairs of these lasers are tagged with a frequency offset such that the satellite is scanned in 2 dimensions by the fringe pattern formed by the laser irradiance at

the satellite. The resulting scan modulation generates a closure phase which can be read by a simple photo detector on the ground. The GLINT concept did not proceed to system level testing.

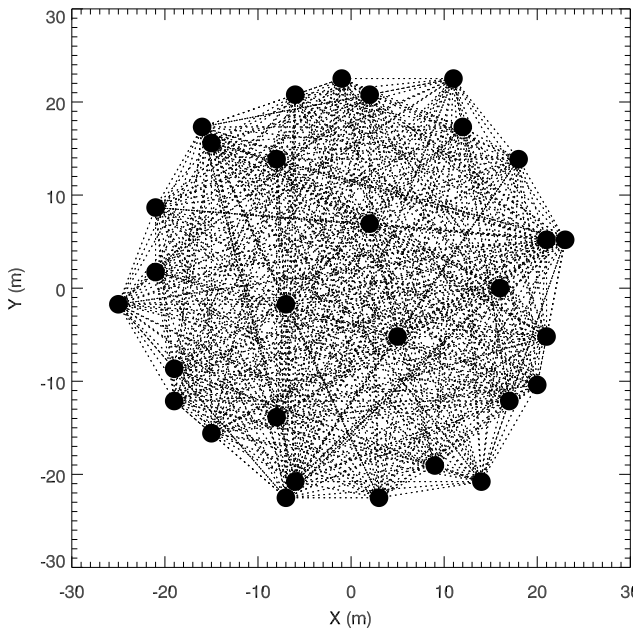


Figure 2. Map of stations and baselines for both the non-redundant array.

2. INSTRUMENT DESCRIPTION

The instrument that we propose is depicted in Figure 1. It consists of a single mount with a size of approximately 50 m (depending on the desired resolution) and approximately 30 telescopes each with a diameter of 1.4 m (depending on the desired sensitivity). In this concept V-band light is used for the wavefront sensor to phase the large mirrors, H-band light is used for fringe-tracking, and the imaging is carried out in the R-band. The companion paper by Mozurkewich et al.¹ describes the instrument and optics in detail.

The telescopes are laid out in a non-redundant array configuration, shown in Figure 2 together with all possible 870 baselines. The light from the telescopes is fed into fibers which transport it to the beam combiner at the center of the telescope. This design has a small number of mirrors and high throughput. Very importantly, the design involves no long delay lines, and no tracking mounts for the individual telescopes, which is likely to reduce the cost of the system, and which also makes it easier to install additional telescopes on the structure. Not having individual mounts on the telescopes also makes it possible to place them closer together to improve fringe-tracking performance. All 870 baselines can be observed simultaneously.

The fringe-tracking system (in H-band) and imaging systems (in R-band) are configured differently. For

Band	λ (μm)	$\frac{\Delta\lambda}{\lambda}$	Flux (Jy)
R	0.64	0.23	3080
H	1.60	0.23	1080

Table 1. Flux from a 0th magnitude satellite in the R- and H-bands. These were obtained from <http://www.astro.utoronto.ca/~patton/astro/mags.html>, which referenced Bessel (1990)¹⁴ as the source for R-band flux and Campins et al. (1985)¹⁵ as the source for the H-band flux.

fringe-tracking it only makes sense to split the light between the baselines which have large SNR. For imaging we want all or most baselines. For combining all baselines there are two basic options, one involving pairwise combination (thus splitting the light in 30), and the other involving all-on-one combiner. The all-on-one combiner has slightly better SNR characteristics. We will however base our calculations on 870 pair-wise combinations because those calculations are straightforward.

3. SIGNAL-TO-NOISE CALCULATIONS

The signal-to-noise ratio for fringe-tracking is

$$\text{SNR}_T = NV^2$$

where N is the number of photons collected across the H-band in one integration and V is the visibility amplitude on the baseline. We take the integration time to be $T = 2\tau_0$ where τ_0 is the atmospheric coherence time, which we assume is $\tau_0 = 3\text{ ms}$ at a wavelength $\lambda_0 = 500\text{ nm}$. At other wavelengths we scale the coherence time according to

$$\tau = \left(\frac{\lambda}{\lambda_0} \right)^{\frac{6}{5}}$$

It is generally agreed that a SNR of a few (e.g. greater than 3, preferably greater than 7) is required for proper fringe-tracking.

For the case of imaging SNR we will assume that the fringe visibilities are coherently integrated,^{3,16,17} and in that case the SNR is

$$\text{SNR}_I = V\sqrt{N}$$

The photon counts are obtained in the following way. Table 1 lists the full-band fluxes (in Jy), the central wavelengths as well as the bandwidths of the channels.

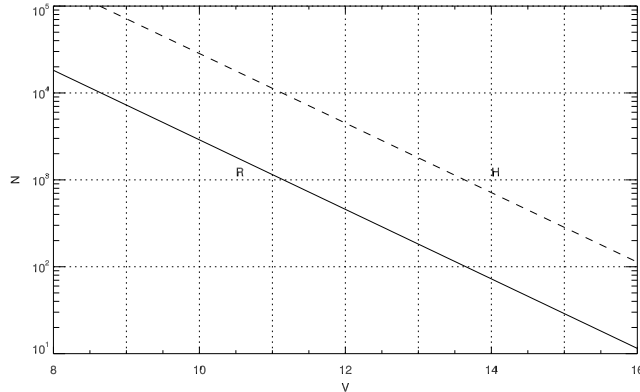


Figure 3. The number of photons reaching the beam combiner in R- and H-bands in two coherence times, assuming $\tau_0 = 3$ ms at 500 nm.

These are converted into photon fluxes at the top of the atmosphere in the following way,

$$N = 1.51 \times 10^7 \times F \times \frac{\Delta\lambda}{\lambda} \times T \times A \times \alpha$$

Where

$$F = F_0 10^{-\frac{m}{2.5}}$$

m is the satellite magnitude, and F_0 is the flux of a $m = 0$ object, in Jy, taken from Table 1, $\frac{\Delta\lambda}{\lambda}$ is the bandwidth which can be anything, for example the full bandpass of each of the astronomical bands (from Table 1), T is the integration time, and A is the area of the telescope entrance aperture. α is the throughput which consists of several components. One is the throughput of the optics, primarily the beam combiner, which we take to be 10%. A second component comes from the imperfect corrections by the adaptive optics system. In general this factor is dependent on the magnitude of the satellite, being smaller for fainter satellites. For simplicity we will use the factor derived by Mozurkewich et al <http://www.astro.utoronto.ca/patton/astro/mags.html>.¹ for a visible magnitude $V=13.5$.

Because we use single-mode fibers, incoherent photons are discarded at the fiber feed rather than resulting in reduced visibility, so that the system visibility should be very close to unity. Here we assume unity system visibility.

The final factor that will need to be considered is the number of times the light is assembled or divided.

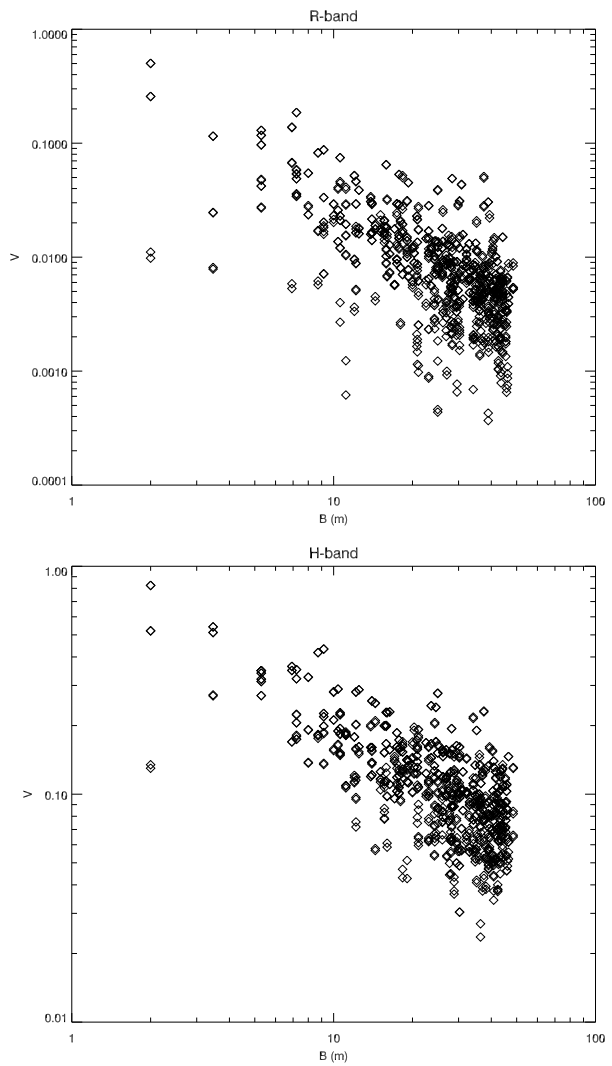


Figure 4. Visibility amplitude as a function of baseline length for (a) $0.64\text{ }\mu\text{m}$, (b) $1.6\text{ }\mu\text{m}$ (estimated, as described in text).

For example one baseline will always be the combination of two beams, and we may divide the light multiple times. If we are doing 30-way pairwise combination we should divide the above numbers by 15 (multiply by 2 and divide by 30). Figure 3 plots the number of photons per telescope that reach the beam combiner in one coherence time (assuming $\tau_0 = 3$ ms) under these assumptions. For $V = 13.5$ it is approximately 110 photons in R-band, and approximately 1100 photons in H-band.

4. SATELLITE VISIBILITIES

For this paper we analyze the visibilities used by Schmitt et al^{2,6} in the satellite imaging studies. Figure 4 shows the visibility amplitudes as a function of

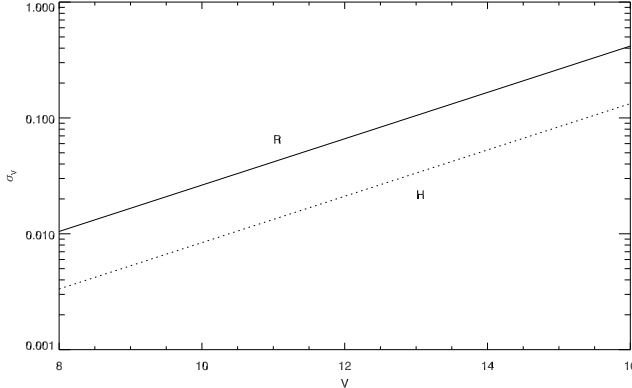


Figure 5. Visibility standard deviation after a integration time of two coherence times when the light is split four ways and combined pairwise for fringe-tracking, for R-band (solid) and H-band (dotted). Using $\tau_0 = 3$ ms, full bandpass in H-band and 300 nm bandpass in R-band.

baseline length in the R-band and in the H-band, with the H-band visibility distribution estimated from the visibilities at $0.8 \mu\text{m}$. We will use the H-band visibilities to estimate the fringe-tracking performance of the instrument and the R-band visibilities to estimate the imaging performance and required integration time of the instrument.

5. FRINGE-TRACKING SNR

The H-band is best for fringe-tracking due to several factors. The visibilities and photon counts are generally larger because of the still high-solar flux at $1.6 \mu\text{m}$, longer wavelength, the larger atmospheric transparency, and the longer coherence time. (See Figures 3 and 4). We assume that for fringe-tracking the light from each telescope is split 4 ways and combined pairwise, with intelligent selection of the pairs. This means that approximately 10% of the baselines will track and will be used to phase the entire array of telescopes and the remaining 90% of the baselines.

Figure 5 shows the standard deviation of the visibility after an integration time of two coherence times (approximately 8 ms in R-band, and 24 ms in H-band). In order for fringe-tracking to be possible the visibility on the tracking baselines must be significantly larger than this uncertainty. Typically a SNR (ratio of visibility to its uncertainty) should be at least 5 or 10 for fringe-tracking to function well. Using information about the visibility uncertainty we can determine which baselines can track, as a function of satellite magnitude.

Figure 6 plots those baselines which have sufficient SNR for fringe tracking. Baselines with $\text{SNR} > 7$ are shown

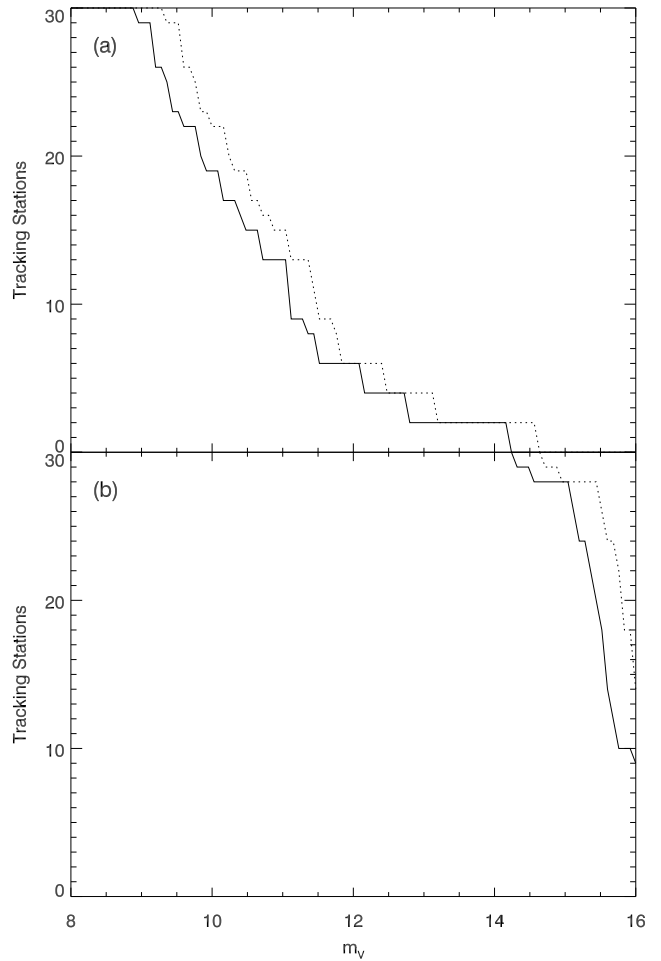


Figure 7. Number of stations connected to a tracking baseline as a function of satellite magnitude in the (a) R-band and (b) H-band. Solid curve represent tracking $\text{SNR} > 10$ and dotted $\text{SNR} > 7$.

as dotted lines, and baselines with $\text{SNR} > 10$ are shown as solid lines. We can see that for $V < 13.5$ many baselines appear to be trackable. Between $V = 13.5$ and $V = 14.5$ many baselines loose trackability, and for $V > 14.5$ only a few baselines remain trackable. We conclude that fringe-tracking is possible approximately to $V = 14.5$.

Another way to illustrate the fringe-tracking limit is given in Figure 7. There we plot the number of stations which are connected to at least one trackable baseline. This gives an indication of the fraction of the array which is phased. Once several stations loose track we can assume that we have effectively reached the limit of fringe-tracking. For the purpose of illustrating the difference between R-band and H-band Figure 7 shows the fringe-tracking capability both in the R-band (top

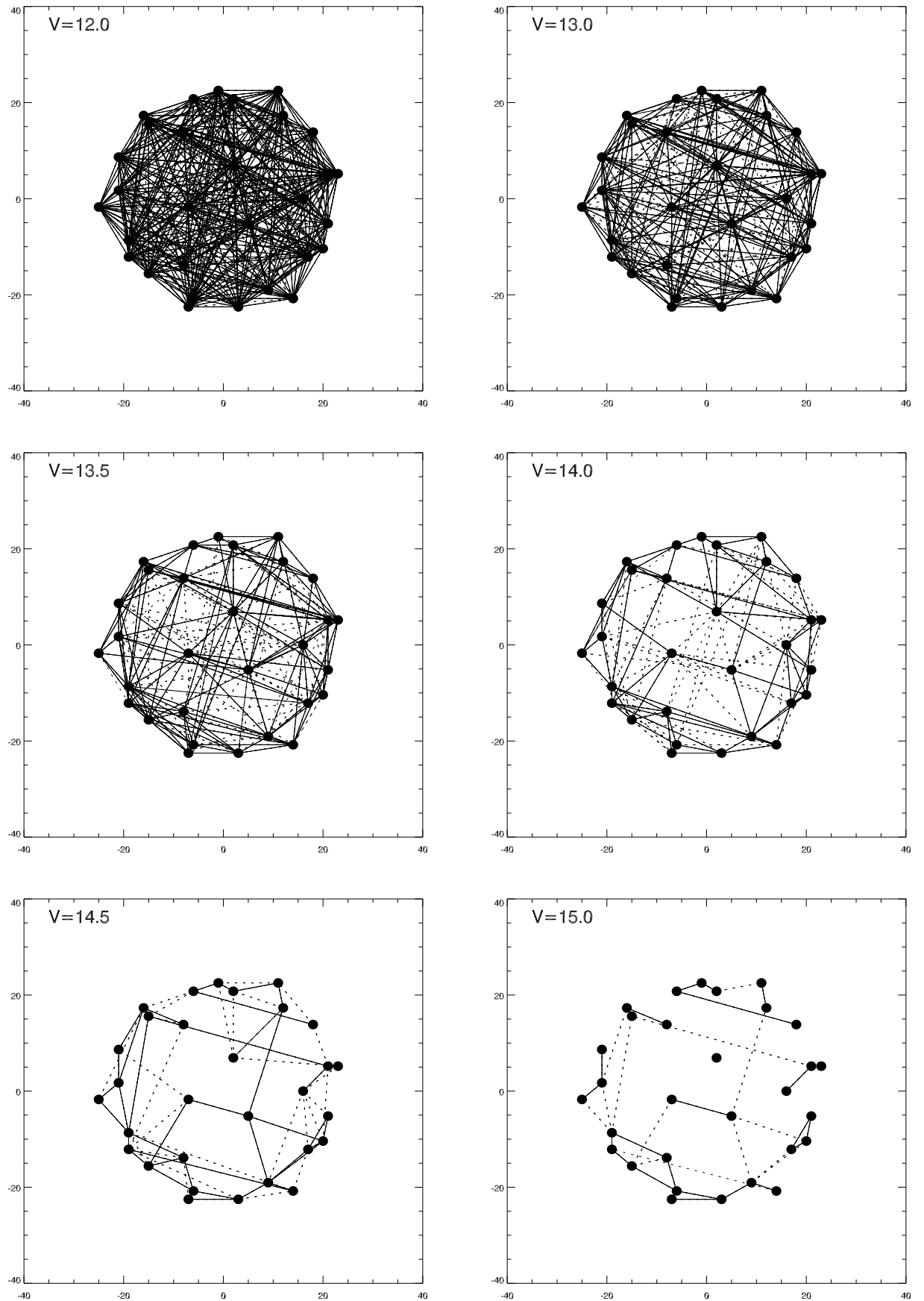


Figure 6. Each panel shows baselines with SNR at least 10 (solid), and 7 (dotted), in H-band, for six different satellite brightnesses. The number of high SNR baselines suggests that the fringe-tracking limit is near $V = 14.5$.

panel) and the H-band (bottom panel). The solid curve plots the number of telescopes connected to a baseline with $\text{SNR} > 10$ and the dotted line the number connected to baselines with $\text{SNR} > 7$. As before we find that fringe-tracking works to approximately $V = 14.5$. By contrast in the R-band fringe-tracking only works to $V = 9$. In the case of the V-band this limit may appear low until one remembers that this is for tracking on the relatively small visibilities plotted in Figure 4.

6. IMAGING SNR

For fringe-tracking it is necessary to obtain sufficient SNR on a small number of baselines which connect the entire array, and to obtain this SNR in a very short amount of time of a few ms. For the purpose of imaging the goal is to obtain a sufficiently large SNR on many or most baselines. Again we can compute the relationship between fringe standard deviation and magnitude, but this time folding in the dimension of integration time.

Figure 8 plots curves of fringe amplitude standard deviation as a function of satellite V-magnitude, giving the corresponding integration time. From this figure we can see that a crude image of a $V = 13.5$ satellite using 10% of the baselines can be recorded in only a few seconds. A more detailed image involving 80% of the baselines can be obtained after less than 30 min integration time.

It should be noted that there are two factors which influence the imaging fidelity. One is the integration time which determines the uncertainty on the visibilities. Another factor is the number and layout of baselines and the extent to which they cover the necessary portions of the UV plane. Once the photon counting noise becomes smaller than the UV coverage noise, additional integration becomes unnecessary. The limit is most likely reached after minutes as opposed to hours of integration, thus making this instrument a minute time-scale snapshot imager. Snapshot imaging is important because it allows for resolving short time-scale changes of the satellite due to maneuvering, changes in sun-angle, or other changes.

7. DISCUSSION

We have presented initial signal-to-noise ratio calculations for a common-mount interferometer consisting of 30 1.4 m telescopes with adaptive optics (in V-band), a fiber-fed fringe-tracker (in H-band), and a fiber-fed imaging combiner (in R-band). We conclude that it is possible to track fringes on typical highly resolved

satellites to a magnitude of $V = 14.5$. This range encompasses the majority of geostationary satellites. It is possible that fringe-tracking can be improved with the addition of a few more telescopes to bridge several long baselines. Adding telescopes to a common-mount interferometer is simpler than adding them to a traditional interferometer because the expense of additional long delay lines does not exist, and because the telescopes are less expensive not having individual mounts. Because the telescopes have no individual mounts they can be placed quite close together as well.

We also found that imaging is possible and that sufficient number of photons can be collected in a few minutes to a few tens of minutes from the majority of the baselines to produce high-fidelity images. This allows for snapshot imaging on the time-scale of minutes which makes it possible to observe a satellite as it maneuvers or as light and shadows transits across it in its orbit.

We believe it may be possible to improve the performance in a few simple ways. While we arrived at a throughput of 10% there are ways in which this can be improved, including using a better adaptive optics system. It is also possible to increase the size of the apertures, for example to 1.8 m diameter, if necessary.

In terms of the mechanical complexity, steerable structures of similar size have been built and used as radio astronomical telescopes. Any vibrations in the structure are likely to be slow enough that they can be compensated by the fringe-tracker and tip-tilt system.

8. CONCLUSION

We have discussed the feasibility of a design for a common-mount many-aperture interferometric telescope for imaging faint resolved sources such as geostationary satellites. We conclude that the instrument as designed is feasible and will indeed be capable of imaging the majority of geostationary satellites in its field of view.

The common-mount interferometer is a useful instrument for imaging faint targets at geostationary orbit. Structures of similar size have been built and used as radio telescopes. The capability to image faint resolved targets at geostationary is bound to have multiple commercial and national security uses including diagnosing costly failures, observing possible enemy satellites, and detecting attempts at compromising own satellites.

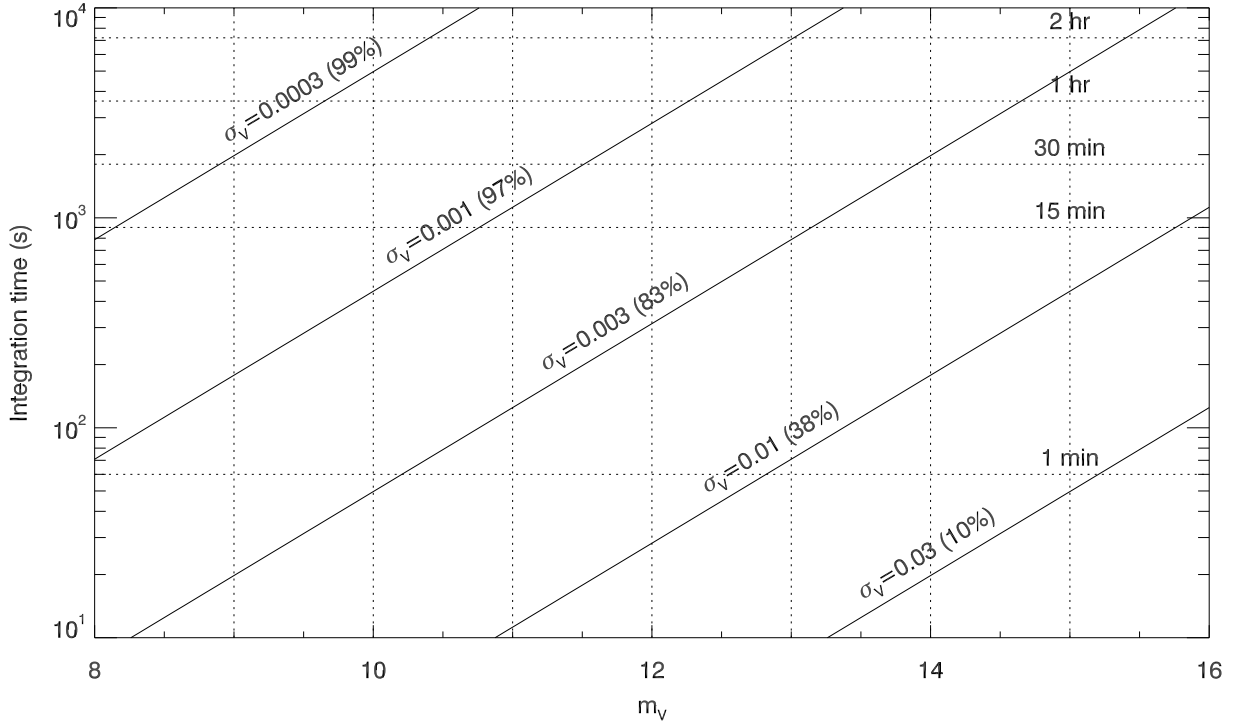


Figure 8. Required R-band integration time as a function of satellite visual magnitude for several different values of fringe standard deviation.

REFERENCES

1. D. Mozurkewich, J. T. Armstrong, R. B. Hindsley, A. M. Jorgensen, S. R. Restaino, and H. R. Schmitt, “Toward the ground-based imaging of satellites at geosynchronous altitude,” in Proc. Advanced Maui Optical and Space Surveillance Technologies Conference, 2011.
2. H. R. Schmitt, D. Mozurkewich, S. R. Restaino, J. T. A. nd Ellyn K. Baines, R. B. Hindsley, and A. M. Jorgensen, “Simulated synthesis imaging of geostationary satellites,” in Proc. Advanced Maui Optical and Space Surveillance Technologies Conference, 2011.
3. A. M. Jorgensen, H. Schmitt, J. T. Armstrong, D. Mozurkewich, E. Baines, R. Hindsley, D. Hutter, and S. Restaino, “Coherent integration results from the NPOI,” in Proceedings of the SPIE meeting Astronomical Telescopes and Instrumentation, 2010.
4. E. J. Bakker, D. A. Klingsmith, A. M. Jorgensen, D. Westpfahl, V. Romero, and C. Cormier, “Imaging of geostationary satellites with the MRO interferometer,” in Proc. Advanced Maui Optical and Space Surveillance Technologies Conference, 2009.
5. D. Mozurkewich, J. T. Armstrong, R. B. Hindsley, A. M. Jorgensen, S. R. Restaino, and H. R. Schmitt, “An imaging interferometer for compact sources,” in Proc. SPIE 8165, 2011.
6. H. R. Schmitt, D. Mozurkewich, S. R. Restaino, J. T. Armstrong, E. K. Baines, R. B. Hindsley, and A. M. Jorgensen, “Simulated optical interferometric observations of satellites,” in Proc. SPIE 8165, 2011.
7. J. T. Armstrong, R. B. Hindsley, S. R. Restaino, J. A. Benson, D. J. Hutter, F. J. Vrba, R. T. Zavala, S. A. Gregory, and H. R. Schmitt, “Observations of a geosynchronous satellite with optical interferometry,” in Proc. Advanced Maui Optical and Space Surveillance Technologies Conference, 2009.
8. D. J. Sanchez, S. A. Gregory, D. K. Werling, T. E. Payne, L. Kann, L. G. Finkner, D. M. Payne, and C. K. Davis, “Photometric measurements of deep space satellites,” in Proc. SPIE 4091, Imaging Technology and Telescopes, J. W. Bilbro, J. B. Breckinridge, R. A. Carreras, S. R. Czyzak, M. J. Eckart, R. D. Fiete, and P. S. Idell, eds., 2000.

9. J. T. Armstrong, D. Mozurkewich, L. J. Rickard, D. J. Hutter, J. A. Benson, P. F. Bowers, N. M. E. II, C. A. Hummel, K. J. Johnston, D. F. Buscher, J. H. C. III, L. Ha, L.-C. Ling, N. M. White, and R. S. Simon, “The navy prototype optical interferometer,” *The Astrophysical Journal* **496**, pp. 550–571, 1998.
10. J. T. Armstrong, R. B. Hindsley, S. R. Restaino, R. T. Zavala, J. A. Benson, F. J. Vrba, D. J. Hutter, S. A. Gregory, H. R. Schmitt, J. R. Andrews, and C. C. Wilcox, “Observations of a geosynchronous satellite with optical interferometry,” in *Adaptive Coded Aperture Imaging, Non-Imaging, and Unconventional Imaging Sensor Systems II*, S. Rogers, D. P. Casasent, J. J. Dolne, T. J. Karr, and V. L. Gamiz, eds., p. 78180L, 2010.
11. J. T. Armstrong, R. B. Hindsley, H. R. Schmitt, F. J. Vrba, J. A. Benson, D. J. Hutter, and R. T. Zavala, “Detection of a geostationary satellite with the Navy Prototype Optical Interferometer,” in *Proc. Optical and Infrared Interferometry II*, W. C. Danchi, F. Delplancke, and J. K. Rajagopal, eds., pp. 77343C–77343C–7, 2010.
12. I. Payne, M. Creech-Eakman, V. Romero, D. Buscher, and C. Haniff, “The magdalena ridge observatory interferometer: Geostationary target imaging capabilities,” in *Proc. Advanced Maui Optical and Space Surveillance Technologies Conference*, 2010.
13. V. J. Gamiz, R. B. Holmes, S. R. Czysak, and D. G. Voelz, “GLINT: program overview and potential science objectives,” in *Proc. SPIE 4091, Imaging Technology and Telescopes*, J. W. Bilbro, J. B. Breckinridge, R. A. Carreras, S. R. Czysak, M. J. Eckart, R. D. Fiete, and P. S. Idell, eds., pp. 304–315, 2000.
14. M. S. Bessel, “UvPRI passbands,” *PASP* **91**, p. 589, 1990.
15. H. Campins, G. H. Reike, and M. J. Lebovsky, “Absolute calibration of photometry at 1 through 5 microns,” *Astronomical Journal* **90**, pp. 896–899, 1985.
16. A. M. Jorgensen, D. Mozurkewich, T. Armstrong, H. Schmitt, C. Gilbreath, R. Hindsley, and T. A. Pauls, “Improved coherent integration through fringe model fitting,” *Astronomical Journal* **134**, pp. 1544–1550, 2007.
17. A. M. Jorgensen, D. Mozurkewich, H. Schmitt, R. Hindsley, J. T. Armstrong, and T. A. Pauls, “Practical coherent integration in optical interferometry,” in *Proceedings of the SPIE Conference* Astronomical Telescopes and instrumentation, 2008.